

**NUCLEAR DATA AND MEASUREMENTS SERIES**

**ANL/NDM-22**

**Note on Neutron Scattering and the Optical Model Near  $A = 208$**

by

P. Guenther, D. Havel, and A. Smith

September 1976

**ARGONNE NATIONAL LABORATORY,  
ARGONNE, ILLINOIS 60439, U.S.A.**

# NUCLEAR DATA AND MEASUREMENTS SERIES

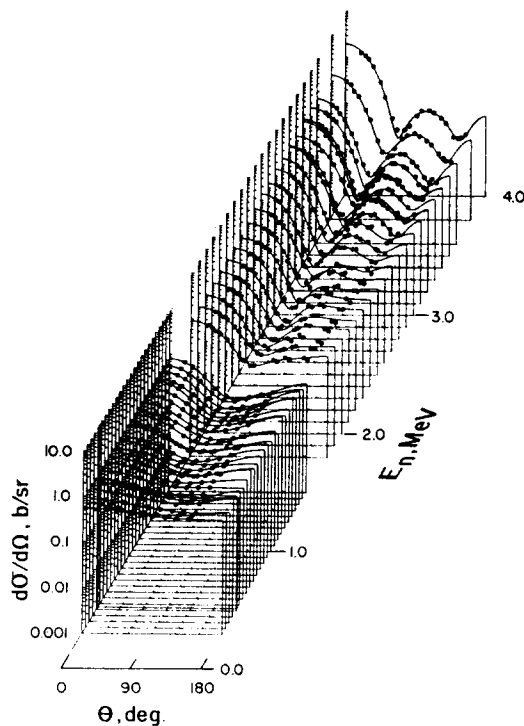
ANL/NDM-22

NOTE ON NEUTRON SCATTERING AND THE  
OPTICAL MODEL NEAR  $A=208^*$

by

P. Guenther, D. Havel and A. Smith

September 1976



ARGONNE NATIONAL LABORATORY,  
ARGONNE, ILLINOIS 60439, U.S.A.

The facilities of Argonne National Laboratory are owned by the United States Government. Under the terms of a contract (W-31-109-Eng-38) between the U. S. Atomic Energy Commission, Argonne Universities Association and The University of Chicago, the University employs the staff and operates the Laboratory in accordance with policies and programs formulated, approved and reviewed by the Association.

#### MEMBERS OF ARGONNE UNIVERSITIES ASSOCIATION

The University of Arizona	Kansas State University	The Ohio State University
Carnegie-Mellon University	The University of Kansas	Ohio University
Case Western Reserve University	Loyola University	The Pennsylvania State University
The University of Chicago	Marquette University	Purdue University
University of Cincinnati	Michigan State University	Saint Louis University
Illinois Institute of Technology	The University of Michigan	Southern Illinois University
University of Illinois	University of Minnesota	The University of Texas at Austin
Indiana University	University of Missouri	Washington University
Iowa State University	Northwestern University	Wayne State University
The University of Iowa	University of Notre Dame	The University of Wisconsin

#### NOTICE

This report was prepared as an account of work sponsored by the United States Government. Neither the United States nor the United States Atomic Energy Commission, nor any of their employees, nor any of their contractors, subcontractors, or their employees, makes any warranty, express or implied, or assumes any legal liability or responsibility for the accuracy, completeness or usefulness of any information, apparatus, product or process disclosed, or represents that its use would not infringe privately-owned rights.

ANL/NDM-22

NOTE ON NEUTRON SCATTERING AND THE  
OPTICAL MODEL NEAR  $A=208^*$

by

P. Guenther, D. Havel and A. Smith

September 1976

In January 1975, the research and development functions of the former U.S. Atomic Energy Commission were incorporated into those of the U.S. Energy Research and Development Administration.

Applied Physics Division  
Argonne National Laboratory  
9700 South Cass Avenue  
Argonne, Illinois 60439  
U.S.A.

## NUCLEAR DATA AND MEASUREMENTS SERIES

The Nuclear Data and Measurements Series presents results of studies in the field of microscopic nuclear data. The primary objective is the dissemination of information in the comprehensive form required for nuclear technology applications. This Series is devoted to:

a) Measured microscopic nuclear parameters, b) Experimental techniques and facilities employed in data measurements, c) The analysis, correlation and interpretation of nuclear data, and d) The evaluation of nuclear data. Contributions to this Series are reviewed to assure technical competence and, unless otherwise stated, the contents can be formally referenced. This Series does not supplant formal journal publication but it does provide the more extensive information required for technological applications (e.g., tabulated numerical data) in a timely manner.

# TABLE OF CONTENTS

	<u>Page</u>
ABSTRACT . . . . .	3
I. INTRODUCTION . . . . .	4
II. EXPERIMENTAL METHODS . . . . .	5
III. EXPERIMENTAL RESULTS . . . . .	6
IV. INTERPRETATION . . . . .	8
V. EXTRAPOLATION TO $^{238}\text{U}$ . . . . .	12
VI. CONCLUDING REMARKS . . . . .	16
REFERENCES . . . . .	18
TABLES . . . . .	20
FIGURE CAPTIONS. . . . .	25

NOTE ON NEUTRON SCATTERING AND THE  
OPTICAL MODEL NEAR  $A=208^*$

by

P. Guenther, D. Havel and A. Smith

ABSTRACT

Elastic neutron scattering cross sections of  $^{206}\text{Pb}$ ,  $^{207}\text{Pb}$ ,  $^{208}\text{Pb}$  and  $^{209}\text{Bi}$  are measured at incident neutron energy intervals of  $\sim 25$  keV from 0.6 to 1.0 MeV with resolutions of  $\sim 25$  keV. Optical model parameters are obtained from the energy-averaged experimental results for each of the isotopes. The observed elastic-neutron-scattering distributions and derived parameters for the lead isotopes (doubly magic or neutron holes in the closed shell) tend to differ from those of  $^{209}\text{Bi}$  (doubly closed shell plus a proton). These potentials, derived in the approximately spherical region of  $A \sim 208$ , are extrapolated for the analysis of total and scattering cross sections of  $^{238}\text{U}$  introducing only a small  $\frac{N-Z}{A}$  dependence and the known deformation of  $^{238}\text{U}$ . Good descriptions of  $^{238}\text{U}$  total cross sections are obtained from a few hundred keV to 10.0 MeV and the prediction of measured scattering distributions in the low MeV region are as suitable as frequently reported with other specially developed potentials.

---

\* This work supported by the U.S. Energy Research and Development Administration.

## I. INTRODUCTION

A physical problem of considerable applied interest is neutron scattering from actinide isotopes, e.g.  $^{238}\text{U}$ . The primary energy range of interest is below several MeV where the fast-breeding-reactor spectrum is concentrated. Direct experimental study of such processes is difficult and as a consequence, they are not precisely known. A good model for the interpolation and extrapolation of difficult-to-measure values is very useful. Such a model must recognize the characteristic deformation of these actinides with additional parameters and complexity that are not well defined by comparisons with the limited experimental data base. Faced with these difficulties it is attractive to separate the model problem with an initial derivation of a simple and precise spherical potential in the context of heavy-spherical nuclei near  $A \sim 208$  and then extend this potential to the actinides using only known deformations and a small  $\frac{N-Z}{A}$  dependence. Nuclei near  $A \sim 208$  have  $\frac{N-Z}{A}$  values very near those of the actinides; e.g.  $^{238}\text{U}$ . The experimental measurement of their elastic scattering cross sections are relatively simple and reasonably free of complexities due to inelastic scattering at incident energies  $\lesssim 1.0$  MeV. Suitable isotopes for such an experimental study are  $^{206}\text{Pb}$ ,  $^{207}\text{Pb}$ ,  $^{208}\text{Pb}$  and  $^{209}\text{Bi}$ . The major experimental problem is the acquisition of a sufficiently wide data base to permit a reasonable derivation of an energy-averaged cross sections consistent with the concept of an optical potential. The total cross sections of the above isotopes are known to fluctuate (1,2). This structure near 1.0 MeV is least severe in the odd isotope  $^{209}\text{Bi}$ , more appreciable in  $^{206}\text{Pb}$  and  $^{207}\text{Pb}$  and very prominent in  $^{208}\text{Pb}$ . For a reasonable average, the data base must extend over at least several hundred keV. At the same time the experimental resolutions and incident energies should be chosen so as to avoid the complexities of inelastic-scattering contributions insofar as possible. For the isotopes  $^{206}\text{Pb}$ ,  $^{207}\text{Pb}$ ,  $^{208}\text{Pb}$  and  $^{209}\text{Bi}$  these experimental conditions can be reasonably met over the incident neutron energy range 0.6 to 1.0 MeV

The above concepts were examined with detailed measurements of the elastic neutron scattering cross sections of  $^{206}\text{Pb}$ ,  $^{207}\text{Pb}$ ,  $^{208}\text{Pb}$ , and  $^{209}\text{Bi}$  from 0.6 to 1.0 MeV and the associated derivation of isotope-dependent optical potentials. The lead results were obtained some time ago but have not been examined in detail or previously reported. Some of the bismuth results were obtained concurrently with the lead values others were obtained independently. All bismuth values have been previously reported (3). The spherical lead and bismuth potentials were explicitly used to calculate  $^{238}\text{U}$  neutron total and scattering cross sections using a coupled-channel method introducing only the reported deformations and a small  $\frac{N-Z}{A}$  dependence (4). These calculated  $^{238}\text{U}$  results are compared with measured values reported in the literature (5,6,7,8).

## II. EXPERIMENTAL METHODS

All data was taken using fast neutron time-of-flight techniques (9). Two forms of the method were employed. The first involved a single detector placed sequentially in angle between  $\sim 20$  and  $\sim 145$  deg. Using this approach measurements were made approximately every 25 keV for incident energies between 0.6 and 1.0 MeV and with an incident resolution of  $\sim 25$  keV referenced to the threshold of the  $^7\text{Li}(p,n)^7\text{Be}$  source reaction. The nominal angular settings were 20, 30, 45, 60, 75, 90, 105, 120, 135 and 145 deg. At each angle  $^{206}\text{Pb}$ ,  $^{207}\text{Pb}$ ,  $^{208}\text{Pb}$  and  $^{209}\text{Bi}$  samples were sequentially measured. The second measurement method employed a multi-angle detector system (10) permitting 8 concurrent measurements at the approximate angles of 28, 38, 43, 61, 76, 114, 129 and 155 deg. This second method was employed only for studies of bismuth. Herein bismuth results obtained using single and multiple detection systems are considered independently and collectively.

The samples were solid metal cylinders approximately 2 cm in diameter and 2 cm long. The bismuth sample was cast of natural metal (i.e.  $^{209}\text{Bi}$ ). The lead samples were isotopically separated to purities of  $\sim 95$  atom-percent.

All measurements employed the  ${}^7\text{Li}(p,n){}^7\text{Be}$  source reaction with the lithium vacuum deposited on thin tantalum backings to a thickness giving the above incident energy resolution. Energy scales were determined using an electrostatic cylindrical capacitor for ion-beam analysis. Scattering angles were determined optically to within  $\sim 2$  deg. Source intensity was monitored to  $\sim 1\%$  using several "long counters" (11). All measurements were made relative to carbon (12) using carbon samples of the same size as the lead and bismuth samples. Results were corrected for beam attenuation and multiple-event effects using a first-order Monte-Carlo procedure (13). This method was limited in accuracy to several percent but was applied uniformly to all samples and the observed distributions were both similar and not particularly anisotropic. Thus any possible distortions due to correction procedures are expected to be smaller than other uncertainties and generally systematically the same for all isotopes. Therefore, the effect of uncertainties in correction procedures should be relatively small between the isotopes of the measurement set.

### III. EXPERIMENTAL RESULTS

The measured differential elastic scattering cross sections of  ${}^{206}\text{Pb}$ ,  ${}^{207}\text{Pb}$ ,  ${}^{208}\text{Pb}$  and  ${}^{209}\text{Bi}$  are summarized in Fig. 1. The statistical accuracies of the individual differential values were  $\sim 1 - 5$  percent. Uncertainties due to correction procedures were 2-5 percent. Normalization uncertainties including those associated with the carbon reference standard were estimated to be 5-8 percent. Thus the collective RMS uncertainties were  $\sim 5-10$  percent. The reproducibility of the data was far better. As noted above, the measurements were made concurrently for all lead samples and many bismuth samples thus systematic distortions will generally effect results in the same way and relative differences between the true values will be largely retained. Fig. 1 clearly shows the expected angular-dependent fluctuations. These are least appar-

ent in  $^{209}\text{Bi}$  and progressively more apparent in  $^{206}\text{Pb}$ ,  $^{207}\text{Pb}$  and, finally,  $^{208}\text{Pb}$ .

The above data base was energy-averaged about 800 keV using the two energy ranges of: 1)  $800 \pm 100$  keV and 2)  $800 \pm 200$  keV. The measured values were obtained at essentially the same scattering angles. Where necessary for averaging, the measured values were interpolated between angles by small amounts using Legendre polynomial fits to the measured values. Nearly a hundred data points were contained within the narrower ( $\pm 100$  keV) average and approximately 175 in the wider ( $\pm 200$  keV) average as noted in Table 1. The experimental values were nearly equally distributed about 800 keV for each isotope as shown in Table 1. The average bismuth energies were slightly different from those of the lead isotopes due to several additional distributions. In addition to the above data sets there was a large amount of 8-angle information for bismuth (3). This was combined with the above 10-angle data to form a separate "augmented" bismuth data set noted in Table 1.

The above average values are illustrated in Fig. 2 together with an unconstrained  $P_4$  Legendre polynomial least-square fit to each distribution. The two averages for  $^{206}\text{Pb}$  are essentially identical in shape and agree in normalization to within several percent. The two  $^{207}\text{Pb}$  average distributions are very nearly identical. There is a pronounced difference between the two average  $^{208}\text{Pb}$  distributions. The two average  $^{209}\text{Bi}$  distributions using the above 10-angle data set have similar shapes but differ by a few percent in normalization. Similar averages for the larger ("augmented")  $^{209}\text{Bi}$  data set are essentially indistinguishable. These averages indicate that for  $^{206}\text{Pb}$ ,  $^{207}\text{Pb}$  and  $^{209}\text{Bi}$  an average obtained over the  $800 \pm 200$  keV range gives a good average representation of the behavior of the differential elastic scattering cross sections at about  $\sim 800$  keV. Such a conclusion is less certain for  $^{208}\text{Pb}$  as the  $\pm 100$  keV and  $\pm 200$  keV averages are considerably different.

The elastic distributions for the above four isotopes are somewhat different as illustrated by the comparison of the results of Legendre fits to the  $\pm 200$  keV-averaged data shown in Fig. 3.  $^{206}\text{Pb}$  and  $^{207}\text{Pb}$  are very similar over the measured angular range.  $^{208}\text{Pb}$  is somewhat different from the other lead isotopes. The distribution for  $^{209}\text{Bi}$  is appreciably different from any of the lead distributions at both forward and back angles. This difference is in excess of that possibly due to relative experimental uncertainties. The present lead measurements can be combined with appropriate isotopic weighting to yield energy-averaged cross sections essentially identical to those of the natural element. These "elemental" values and the present bismuth results can then be compared with the broad resolution results of Langsdorf et al. (12). The latter are total scattering distributions but in this mass-energy region they should be very similar to elastic scattering distributions. The Langsdorf et al. results were read from the large coefficient curves of ANL-5567 every 30 keV from 0.6 to 0.96 MeV, the corresponding cross sections constructed and then averaged in the same manner as the present data. These averages of the Langsdorf et al. results for natural lead and bismuth are compared with the  $\pm 200$  keV averages of the present work in Fig. 4. The agreement is judged to be very good. Moreover, the average Langsdorf et al. values again clearly show the systematic differences between bismuth and lead distributions.

#### IV. INTERPRETATION

The above averaged experimental results were interpreted in terms of a spherical optical potential consisting of: a saxon real term, a saxon-derivative imaginary term, and a Thomas spin-orbit term (14). The two averages of the experimental results ( $\pm 100$  and  $\pm 200$  keV) were treated independently for each isotope. In addition, the two  $^{209}\text{Bi}$  data sets (10-angle and augmented) were treated separately. Compound-nucleus processes were calculated using the Hauser-Feshbach formula with width fluctuation correc-

tions (15). At 800 keV, scattering from  $^{208}\text{Pb}$  is entirely elastic.  $^{209}\text{Bi}$  has an excited state at 897 keV (16). However, the corresponding inelastic scattering cross section at energies of  $< 1.0$  MeV is known to be small (3) and there was little difference between  $\pm 100$  and  $\pm 200$  keV averages of measured values. The inelastic scattering events could not have contributed to the former average. Therefore  $^{209}\text{Bi}$  scattering was assumed to be entirely elastic.  $^{206}\text{Pb}$  has an excited state at 803 keV (16). The corresponding inelastic scattering could be a factor in both  $\pm 100$  and  $\pm 200$  keV averages of experimental values but relatively much larger in the latter. The two experimental average distributions were very similar therefore it was assumed that scattering from  $^{206}\text{Pb}$  was entirely due to elastic processes.  $^{207}\text{Pb}$  has excited states at 569 and 898 keV (16). The inelastic scattering due to the latter will have little effect on the  $\pm 200$  keV average of the experimental values and none on the  $\pm 100$  keV average. Therefore the 898 keV level was not considered in the calculations. Inelastic scattering due to the excitation of 569 keV state of  $^{207}\text{Pb}$  will have an influence over the entire measured energy interval therefore this state was explicitly included in the calculations. The corresponding inelastic-neutron scattering cross sections were not negligible (e.g.  $\sim \frac{1}{2}$  b).

The six optical model parameters (real and imaginary strengths, radii and diffusenesses) were adjusted to obtain an optimum description of each of the measured energy-averaged distributions using  $\chi^2$ -square fitting procedures (17). The latter involved a random direction parameter search to within specified convergence limits. These limits were set so that generally half the attempts failed to achieve convergence. Sufficient trials were made to obtain five convergent trials for each case. The average deviation of the resulting parameters from the mean was taken as a relative measure of parameter uncertainty. Parameters derived from convergent calculations did not differ greatly from those resulting from non-convergent results. The parameter results from these fitting

procedures are summarized in Table 2. This table also gives the average parameter values obtained from all fits regardless of convergence (as many as 16 attempts in one instance).

The  $^{209}\text{Bi}$  parameter values were generally a factor of two more precise than those obtained for the lead isotopes, with the smallest deviations associated with the larger data sets and wider averaging increments. The  $^{209}\text{Bi}$  results were all very similar indicating a reasonable average representation was achieved. The quality of the model parameters is further indicated by the comparisons of measured and calculated distributions shown in Fig. 5. The average deviation of measured from calculated values was  $\sim 2\%$  for all  $^{209}\text{Bi}$  distributions. The calculated total cross section was in reasonable agreement with that reported from experiments (1).

The parameters obtained from the two  $^{206}\text{Pb}$  averages are essentially the same as indicated in Table 2. However, the average parameter deviations and the average deviation of measured quantities from calculated values (see Fig. 5) are more than a factor of two larger than for  $^{209}\text{Bi}$ . This larger uncertainty may reflect some residual fluctuations even in the  $\pm 200$  keV average.

The character of the  $^{207}\text{Pb}$  fits to the data is very similar to that of the  $^{206}\text{Pb}$  case (see Table 2 and Fig. 5). However, the average deviation of the measured quantities from the calculated values is a factor of 1.5 - 2.0 larger and the calculated distributions are qualitatively discrepant with measurements at a few angles. In addition, in this  $^{207}\text{Pb}$  case there is the concern for the appropriateness of the treatment of the prominent inelastic scattering component. The odd isotope,  $^{207}\text{Pb}$  would be expected to provide a better average than the even  $^{206}\text{Pb}$  but it is not clearly so.

The modeling of  $^{208}\text{Pb}$  was least appropriate. The average deviations of the parameters were the largest of the set (approximately four times some of those of  $^{209}\text{Bi}$ ) and the deviation of the measured average from the calculated values was the largest (see Table 2 and Fig. 5). These factors and the qualitative

differences between  $^{208}\text{Pb} \pm 100$  keV and  $\pm 200$  keV averages, shown in Fig. 2, suggest that the measured averages did not provide a particularly good average representation of  $^{208}\text{Pb}$  scattering.

The parameters of Table 2 seem to show an isotopic dependence. This is illustrated for both  $\pm 100$  and  $\pm 200$  average results in Fig. 6. The average deviations in the real parameters ( $V$ ) of the lead isotopes are large but there is a trend for the real potential magnitudes to be systematically lower than the much better defined  $^{209}\text{Bi}$  value by about 1.0 MeV. Moreover, the illustrated average deviations may be a conservative estimate of uncertainty as the consistency of the real potential magnitudes between different averages of the lead isotope results is appreciably better. Perhaps a better indication of real potential strength is the product  $VR^2$  (14). This product is plotted as a function of isotope in Fig. 7 including the natural lead value inferred from the present measurements. The same general isotopic trends of Fig. 6 are again evident in Fig. 7. The product  $VR^2$  decreases as the double shell closure at 208 is approached in a relatively smooth manner for  $^{206}\text{Pb}$ ,  $^{207}\text{Pb}$  and  $^{208}\text{Pb}$ . There is a well known  $\frac{N-Z}{A}V_0$  dependence of the real potential where  $V_0$  is approximately - 25 MeV (4). Such a trend is consistent with the general observed trend in the lead isotopes but about an order of magnitude too small and does not account for the apparent increase in  $V$  going from the lead isotopes to  $^{209}\text{Bi}$ . It is also suggested by Fig. 7 that the trend in real potential strength is not toward a symmetric minimum at the 208 shell closure but rather toward a "saw tooth" effect. Thus if the observed averages in the present experiments are representative of the energy-averaged behavior near 800 keV; Figs. 6 and 7 are suggestive of differences in the optical potential depending upon whether protons or neutron holes are added to the doubly closed shell at  $A=208$ . Alternatively, a charge-dependent core polarization effect may be present. Bismuth distributions were calculated assuming a vibrational interaction with a wide range of interaction strengths. At 800 keV the results

were not significantly different from those obtained assuming spheridicity though there was a noticeable effect at higher energies.

It would be interesting to search for a similar shell dependence of the real potential strength at other energies, particularly very high ( $\sim 8$  MeV) energies where the elastic scattering can be reasonably approximated by optical-model shape scattering.

#### V. EXTRAPOLATION TO $^{238}\text{U}$

The above potentials, based upon experimental results near  $A=208$  and  $E_n = 800$  keV, were extrapolated to  $^{238}\text{U}$  assuming that the real and imaginary potential strengths are given by

$$V_{\text{real}} = V_0 - V_1 \cdot \frac{N-Z}{A} - V_2 \cdot E(\text{MeV})$$

$$W_{\text{imag.}} = W_0 + W_2 \cdot E(\text{MeV})$$
(1)

$V_1$  was assumed to be 25 MeV, approximately the value reported in the literature (4, 14). The results are not sensitive to  $V_1$  as  $\frac{N-Z}{A}$  of  $^{238}\text{U}$  is not very different from that of the lead isotopes and bismuth, (e.g. = 0.212 for  $^{208}\text{Pb}$  and = 0.227 for  $^{238}\text{U}$ ).  $V_2$  was assumed to be 0.3 MeV. This value is reasonably consistent with that reported in the literature (18,19,20,21). The bismuth and lead potentials, as derived above, give no guidance as to  $W_2$ . However, Holmqvist and Wiedling have reported measured bismuth elastic scattering cross sections to  $\sim 8.0$  MeV (22). Comparison of the results of calculations using the above bismuth model with these measured high-energy distributions indicated suitable  $W_2$  values of  $\sim +0.4$  MeV as suggested by, for example, LaGrange (19). Using this value and the above bismuth parameters the calculated 8.05 MeV bismuth distribution was qualitatively descriptive of the measured Holmqvist and Wiedling values as shown in Fig. 8,

and not very different from the results obtained by the latter authors by means of explicit parameter fitting to high energy bismuth distributions. The differences between spherical calculation and experiment can reasonably be attributed to vibrational effects in the  $^{209}\text{Bi}$  nucleus at these energies. The known static deformation of  $^{238}\text{U}$  was described by  $\beta_2 = 0.216$  and  $\beta_4 = 0.064$  as given by LaGrange (19) and Möller (23). The bismuth and lead isotopes were assumed spherical. The deformation of  $^{238}\text{U}$  was introduced into the calculations using the coupled-channel computational code JUPITOR (24). At low energies (e.g. 500 keV) the  $^{238}\text{U}$  compound-nucleus contributions were calculated using the code 2-PLUS (25). The calculations extended from low energies (e.g. 500 keV) where the compound-nucleus contributions can be reasonably estimated and to higher energies (e.g. 3.0 MeV) where the elastic processes can be reasonably described by "shape scattering". Aside from the essential introduction of the deformation concept, all parameters of the model were taken explicitly from Table 2 via Eq.1. There were no adjustments. The  $^{209}\text{Bi}$  potential was the best defined of the above four; therefore attention was focused upon its extrapolation to  $^{238}\text{U}$ . For comparison purposes, similar  $^{238}\text{U}$  results were obtained using the model of LaGrange (19). The LaGrange potential and the above  $^{209}\text{Bi}$  potential are defined in Table 3. The major differences between the two potentials are in their radii and diffusenesses. The present  $^{209}\text{Bi}$ -based model is characterized by smaller radii and larger diffusenesses. The results of  $^{238}\text{U}$  calculations were compared with selected experimental values particularly those of Barnard et al. (5), Smith and Guenther (6), Batchelor et al. (7) and with the total cross section as summarized by ENDF/B-IV (8).

Initially, the total neutron cross sections of  $^{238}\text{U}$  were calculated at a number of energies to 15 MeV. Above 0.5 MeV the results obtained with the above  $^{209}\text{Bi}$  potential agreed with the measured values of Schwartz et al. (1) and ENDF/B-IV to within several percent or less as shown in Table 4. The results are very similar to the calculated results of LaGrange (19). This indicates that the

real potential strength is reasonably suitable. At low energies (few hundred keV and less) the present potential gives total cross sections and strength functions larger than those reported from experiment. This can be largely corrected by reducing  $W_0$  of Eq.1 in the manner of LaGrange of Newstead et al. (19,21) but such adjustments are not in the spirit of this study and may degrade the comparisons of measured and calculated elastic distributions at higher energies (e.g. near 500 - 1000 keV).

Primary comparison of measured and calculated  $^{238}\text{U}$  neutron-scattering distributions was made at 0.55 MeV. Here the experimental definition is good, previously suggested models have had their shortcomings and no large energy extrapolation of the bismuth-based potential is necessary. However, the calculations are complicated by large compound-nucleus contributions. The latter are not well understood in this context; particularly as to the correlation enhancement of the elastic channel (26). In the present calculations the total compound-nucleus reaction cross section was fixed by the respective potentials. The relative individual compound nucleus components were calculated using the simpler coupled channel computer program 2-PLUS. The normalizations of the compound-inelastic (45 keV state) and compound-elastic components were adjusted to force a 90 deg. inelastic (45 keV, 2+) cross section of 140 mb/sr inclusive of the direct component as indicated by measurements (5,6). Small corrections were applied for contributions due to the excitation of the 4+(148 keV) state and the radiative capture process. With the model-fixed overall reaction cross section this normalization procedure also determines the compound-elastic component. The normalization constant for the inelastic compound-nucleus component was 0.75. This implies an approximately 25 percent correlation enhancement of the compound elastic component which is well within magnitudes due to the correlation of partial channel widths (26). Calculated results obtained with the bismuth-based potential and that of LaGrange are compared with the measured differential elastic and inelastic scattering cross sections of Barnard et al. (5) and

Guenther et al. (6) in Fig. 9. Neither of the calculational results indicate as much forward-angle inelastic scattering as observed experimentally. The forward-angle cross sections are experimentally difficult but probably not as systematically too large as suggested by calculation. The discrepancy cannot easily be alleviated with parameter adjustments or by modifying the nature of the interaction. Such adjustments are not the intent of this study and a few that were attempted led to problems at other energies. In any event, the distribution of the 45 keV inelastic neutron group is very nearly isotropic and use of either calculated or measured angular distributions for converting isolated angular measurements near  $90^\circ$  to angle-integrated cross sections will give approximately the same result. Both calculations of the elastic scattering distributions at 0.55 MeV are qualitatively in agreement with measurements. The result obtained with the present  $^{209}\text{Bi}$ -based potential, however, give a better quantitative description particularly at back angles. The differences between the two calculations are probably more than those associated with uncertainties in the calculation of compound-elastic contributions. Thus, the  $^{209}\text{Bi}$ -based potential developed in a similar energy and a spherical-nucleus context provides a reasonably satisfying basis for extrapolation into the deformed actinide region at low energies without adjustment of the basic six optical potential parameters. The major limitation of the above approach at these low energies is probably associated with the treatment of the relatively large compound-nucleus components. Complex channel-channel correlations of resonance amplitudes and, to a lesser extent, level-level correlations have not been explicitly treated to the possible detriment of the calculations (26).

The above model was extrapolated to the much higher energy of 3.0 MeV and detailed differential elastic and inelastic cross sections were calculated (for the  $E_x = 45$  (2+) and 148 (4+) keV states). At this energy it is reasonable to assume that these distributions are entirely due to direct reactions. Available measured "elastic" scattering actually consists of the true elastic

component plus at least the contribution due to the inelastic excitation of the 0.045 (2+) state. Assuming this composite distribution, the results calculated with the above  $^{209}\text{Bi}$  potential are in reasonable agreement with the experimental results of Guenther and Smith (6) and Batchelor et al. (7) as illustrated in Fig. 10. Indeed, the agreement at some angles may be better than that obtained with the potential of Ref. 19, specially developed for the treatment of heavy deformed nuclei. Neither calculational result describes all details of the measured values. This is particularly so at large scattering angles. This discrepancy is alleviated at somewhat lower energies. Specifically, the recent very good resolution results of Haouat et al. (27) at 2.5 MeV are better described by both potentials than is the case for the above 3.0 MeV example. Differential cross sections for the 45 keV (2+) and 148 keV (4+) states of  $^{238}\text{U}$  calculated with the above bismuth-based potential were reasonably descriptive of experimental results at 2.5 and 3.0 MeV (6,27,28); within the spread of the measurements from various laboratories. Thus it is reasonable to use the model for extrapolating differential inelastic-scattering values to angle-integrated cross sections.

## VI. CONCLUDING REMARKS

Averages of measured elastic neutron scattering cross sections of  $^{206}\text{Pb}$ ,  $^{207}\text{Pb}$ ,  $^{208}\text{Pb}$  and  $^{209}\text{Bi}$  from 0.6-1.0 MeV were used to determine the parameters of respective spherical optical potentials. The energy-average scattering distributions at  $\bar{E}_n = 800$  were well defined for  $^{209}\text{Bi}$  and, possibly, progressively less so for  $^{206}\text{Pb}$ ,  $^{207}\text{Pb}$  and  $^{208}\text{Pb}$ . Assuming the average representation is valid, the real potential strength appears to be at a minimum at the double shell closure of  $^{208}\text{Pb}$ . Moreover, there is a trend for a difference between potentials applicable to  $A=208$  plus a proton and to  $A=208$  minus a neutron(s). The  $^{209}\text{Bi}$  potential was extrapolated to  $^{238}\text{U}$  assuming a very small  $\frac{N-Z}{A}$  dependence and a  $\beta_2$  and  $\beta_4$  deformation, with all other parameters fixed to the  $^{209}\text{Bi}$  values. The resulting

calculated  $^{238}\text{U}$  total cross sections were in very good agreement with measured values from  $\sim 0.5$  to 15 MeV. Calculated angular distributions of elastic and inelastic neutrons scattered from  $^{238}\text{U}$  were descriptive of measured values reported in the literature at 0.55 MeV and, to a lesser extent, of measurements in the 2.5-3.0 MeV range. The bismuth-based model was less suitable for  $^{238}\text{U}$  at very low energies ( $\lesssim 100$  keV). Specific parameter adjustments could alleviate these shortcomings but were not in the spirit of an explicit extrapolation of the model from spherical to deformed heavy nuclei. In many aspects this physically attractive extrapolation led to calculated results for  $^{238}\text{U}$  in as good agreement as those obtained with models specifically tailored to deformed heavy nuclei.

## REFERENCES

1. R. Schwartz, R. Schrack and H. Heaton, Nat. Bur. Stds. Pub., NBS-138 (1974).
2. S. Cierjacks, P. Forti, D. Kopsch, L. Kropp, J. Nabe and H. Unseld, Instit. Für Angewandte Kernphysik Karlsruhe Report, KFK-1000 (1968).
3. A. Smith et al., Nucl. Sci. and Eng., 41 63 (1970).
4. F. Becchetti and G. Greenlees, Phys. Rev., 182 1190 (1969).
5. E. Barnard, A. Ferguson, W. McMurray and I. van Heerden, Nucl. Phys., 80 46 (1966).
6. A. Smith, Nucl. Phys., 47 633 (1963), See also Guenther et al., Argonne Natl. Lab. Report ANL/NDM-16 (1975).
7. R. Batchelor, W. Gilboy and J. Towle, Nucl. Phys., 65 236 (1965).
8. Evaluated Nuclear Data File B, Version IV, National Neutron Cross Section Center, Brookhaven National Laboratory.
9. L. Cranberg and J. Levin, Los Alamos Scientific Laboratory Report, LA-2177 (1958).
10. A. Smith et al., Nucl. Instr. and Methods, 50 277 (1967).
11. A. Hanson and J. McKibben, Phys. Rev., 72 673 (1974).
12. A. Langsdorf, R. Lane and J. Monahan, Argonne National Laboratory Report, ANL-5567 (Rev.) (1961).
13. G. Duffey, S. Buccino and A. Smith, Argonne National Laboratory Report, Unpublished (1966).
14. P. Hodgson, The Optical Model of Elastic Scattering, Clarendon Press, Oxford (1963).
15. P. A. Moldauer, Rev. Mod. Phys., 36 1079 (1964).
16. Nuclear Data Sheets: A=206, K. K. Seth; A=207, M. Schmorak and R. Auble; A=208, M. B. Lewis; and A=209, M. J. Martin. Nuclear Data Project, Oak Ridge National Laboratory, Oak Ridge, Tenn.
17. P. Moldauer, C. Engelbrecht and G. Duffey, Argonne National Laboratory Report, ANL-6978 (1964); See also E. Auerbach, Brookhaven National Laboratory Report, BNL-6562 (1962).
18. C. Engelbrecht and H. Fiedeldey, Ann. Physics, 42 262 (1967).
19. Ch. LaGrange, NEANDC Report, JAERI-M-5984 (1975).
20. F. Perey and B. Buck, Nucl. Phys., 32 353 (1962).

21. C. Newstead and S. Cierjacks, NEANDC Report, JAERI-M-5984 (NEANDC(J)-38L).
22. B. Holmqvist and T. Wiedling, Aktiebolaget Atomenergi Report, AE-430 (1971).
23. P. Möller, Nucl. Phys., A192 529 (1972).
24. T. Tamura, Oak Ridge National Laboratory Report, ORNL-4132 (1967).
25. C. Dunford, Atomics Inter. Report, NAA-SR-11706 (1966).
26. P. Moldauer, Proc. of the Inter. Conf. on the Study of Nuclear Structure with Neutrons, Paper ME-1, Univ. of Lowell (1976).
27. G. Haouat et al., to be published.
28. T. Marcella et al., private communication.

TABLE 1

## Data Base

	$^{206}_{\text{Pb}}$	$^{207}_{\text{Pb}}$	$^{208}_{\text{Pb}}$	$^{209}_{\text{Bi}}$
$\pm 100$ keV AVE.				
No. Values	92	91	91	90 (178) <sup>a</sup>
Ave. Energy (keV)	798	798	798	806 (813) <sup>a</sup>
$\pm 200$ keV AVE.				
No. Values	176	174	186	160 (441) <sup>a</sup>
Ave. Energy (keV)	797	797	797	792 (826) <sup>a</sup>

a. Values for the "augmented" bismuth data set.

TABLE 2

## Results of Xi-Square Fitting

Isotope/Energy	$V^a$	$W^a$	$R_V$	$R_W$	$a_v$	$a_w$
Pb - 206						
$\bar{E}=797$ keV (600-1000 keV)	46.616 $\pm 0.517$ (46.83	4.018 $\pm 0.362$ 4.365	1.216 $\pm 0.007$ 1.208	1.184 $\pm 0.053$ 1.179	0.824 $\pm 0.059$ 0.852	0.576 0.039 0.569) <sup>b</sup> <sub>11</sub>
	$VR^2 = 68.898 \pm 1.033$					
$\bar{E}=798$ keV (700-900 keV)	46.553 $\pm 0.550$ (46.716	4.079 $\pm 0.222$ 3.931	1.217 $\pm 0.007$ 1.214	1.178 $\pm 0.034$ 1.180	0.848 $\pm 0.048$ 0.854	0.579 $\pm 0.030$ 0.591) <sup>b</sup> <sub>10</sub>
	$VR^2 = 68.945 \pm 1.055$					
Pb - 207						
$\bar{E}=797$ keV (600-1000 keV)	46.525 $\pm 0.393$ (46.605	4.331 $\pm 0.419$ 4.365	1.210 $\pm 0.007$ 1.208	1.166 $\pm 0.042$ 1.179	0.837 $\pm 0.065$ 0.852	0.581 $\pm 0.053$ 0.569) <sup>b</sup> <sub>11</sub>
	$VR^2 = 68.112 \pm 0.78$					
$\bar{E}=798$ keV (700-900 keV)	46.837 $\pm 0.502$ (46.712	4.416 $\pm 0.439$ 4.206	1.209 $\pm 0.003$ 1.206	1.150 $\pm 0.028$ 1.146	0.813 $\pm 0.074$ 0.848	0.579 $\pm 0.043$ 0.592) <sup>b</sup> <sub>9</sub>
	$VR^2 = 68.457 \pm 0.78$					

a. Potential strengths V and W in MeV; radii, R, and diffusenesses, a, in F.

b. Average of all fits regardless of convergence. Subscript denotes number of attempts.

TABLE 2 (Contd.)

Isotope/Energy	$V^a$	$W^a$	$R_V$	$R_W$	$a_v$	$a_w$
Pb-208						
$\bar{E}=786$ keV (600-1000 keV)	47.077 $\pm 0.748$ (46.745	3.999 $\pm 0.750$ 3.605	1.201 $\pm 0.007$ 1.201	1.171 $\pm 0.041$ 1.184	0.805 $\pm 0.100$ 0.849	0.501 $\pm 0.087$ 0.510) <sub>16</sub> $VR^2 = 67.885 \pm 1.18$
$\bar{E}=798$ keV (700-900 keV)	46.759 $\pm 0.829$ (46.536	4.326 $\pm 0.476$ 4.230	1.198 $\pm 0.008$ 1.194	1.215 $\pm 0.041$ 1.221	0.854 $\pm 0.109$ 0.906	0.593 $\pm 0.077$ 0.549) <sub>13</sub> $VR^2 = 67.108 \pm 1.26$
Bi-209 (All data)						
$\bar{E}=826$ keV (600-1000 keV)	47.502 $\pm 0.171$ (47.277	4.032 $\pm 0.326$ 3.985	1.213 $\pm 0.002$ 1.217	1.198 $\pm 0.027$ 1.209	0.757 $\pm 0.014$ 0.753	0.507 $\pm 0.027$ 0.505) <sub>8</sub> $VR^2 = 69.875 \pm 0.580$
$\bar{E}=813$ keV (700-900 keV)	47.593 $\pm 0.296$ (47.595	3.836 $\pm 0.290$ 3.801	1.211 $\pm 0.002$ 1.211	1.204 $\pm 0.029$ 1.210	0.752 $\pm 0.014$ 0.750	0.507 $\pm 0.020$ 0.493) <sub>7</sub> $VR^2 = 69.790 \pm 0.552$
Bi-209 (10-angle data)						
$\bar{E}=792$ keV (600-1000 keV)	47.435 $\pm 0.243$ (47.354	4.047 $\pm 0.222$ 4.259	1.208 $\pm 0.002$ 1.208	1.197 $\pm 0.024$ 1.192	0.757 $\pm 0.014$ 0.761	0.505 $\pm 0.013$ 0.488) <sub>7</sub> $VR^2 = 69.207 \pm 0.519$
$\bar{E}=806$ keV (700-900 keV)	47.593 $\pm 0.306$ (as above, all converged	3.869 $\pm 0.286$ (as above, all converged	1.209 $\pm 0.002$ (as above, all converged	1.192 $\pm 0.025$ (as above, all converged	0.752 $\pm 0.010$ (as above, all converged	0.487 $\pm 0.011$ (as above, all converged) <sub>5</sub> $VR^2 = 69.562 \pm 0.82$

TABLE 3

 $^{238}\text{U}$  Optical Parameters $^{209}\text{Bi}$  Based Potential<sup>a</sup>

$$V(\text{MeV}) = 47.183 - 0.3 E(\text{MeV})$$

$$R_o = 1.211 F$$

$$a = 0.757 F$$

$$W(\text{MeV}) = 4.105 + 0.4 E(\text{MeV})$$

$$R_o = 1.197 F$$

$$a = 0.506 F$$

$$V_{so}(\text{MeV}) = 8.0$$

LaGrange Potential (19)<sup>a</sup>

$$V(\text{MeV}) = 47.5 - 0.3 E(\text{MeV})$$

$$R_o = 1.24 F$$

$$a = 0.62 F$$

$$W(\text{MeV}) = 2.7 + 0.4 E(\text{MeV})$$

$$R_o = 1.26 F$$

$$a = 0.58 F$$

$$V_{so}(\text{MeV}) = 7.5$$

- a. Saxon real form, Saxon-derivative imaginary form, Thomas spin-orbit term.  $\beta_2 = 0.216$ ,  $\beta_4 = 0.064$ ,  $R = R_o A^{1/3}$

TABLE 4

Calculated and Measured Total Cross Sections of  $^{238}\text{U}$ 

E(MeV)	Cal. This <sup>a</sup> Pot. (b)	Cal. Pot. <sup>a</sup> of Ref.19 (b)	Exp(ENDF,Ref.8) (b)
0.20	11.56(6.3%)	10.85 (0.1%)	10.87
0.55	8.45 (0.6%)	8.31 (1.1%)	8.41
1.00	7.17 (0.0%)	7.09 (1.2%)	7.18
2.10	7.49 (3.0%)	7.48 (2.8%)	7.27
3.00	7.98 (1.7%)	7.92 (1.0%)	7.84
5.00	7.61 (0.6%)	7.49 (2.2%)	7.66
10.00	5.88 (0.3%)	5.89 (0.2%)	5.90
15.00	5.71 (4.1%)	5.69 (4.5%)	5.96

a. Percentage deviations are  $\left| \frac{\text{Cal-ENDF}}{\text{ENDF}} \right|$ .

# FIGURE CAPTIONS

Fig. 1. Measured differential elastic scattering cross sections of  $^{206}\text{Pb}$ ,  $^{207}\text{Pb}$ ,  $^{208}\text{Pb}$  and  $^{209}\text{Bi}$ . Data values are indicated by circular points. Curves are the result of unconstrained  $P_4$  fits of a Legendre expansion to the data.

(Neg. No. SFN 22-1)

Fig. 2. Energy-averaged measured differential elastic cross sections of  $^{206}\text{Pb}$ ,  $^{207}\text{Pb}$ ,  $^{208}\text{Pb}$  and  $^{209}\text{Bi}$ .  $\pm 200$  keV averages are indicated by  $\bigcirc$ ,  $\pm 100$  keV averages by  $\times$ . Curves are unconstrained  $P_4$  Legendre fits to the data. The average energy is  $\sim 800$  keV.

(Neg. ANL No. 116-76-240)

Fig. 3. Comparisons of Legendre polynomial fits to the  $\pm 200$  keV averages of the  $^{206}\text{Pb}$ ,  $^{207}\text{Pb}$ ,  $^{208}\text{Pb}$  and  $^{209}\text{Bi}$  elastic scattering data near  $E_n \sim 800$  keV.

(Neg. ANL No. 116-76-133)

Fig. 4. Comparison of  $\pm 200$  keV averages of the present "elemental" lead and bismuth results (data points) with those of Langsdorf et al. (12) (curves).

(Neg. ANL No. 116-76-237).

Fig. 5. Comparison of measured (data points) and model-calculated (curves) elastic scattering distributions of  $^{206}\text{Pb}$ ,  $^{207}\text{Pb}$ ,  $^{208}\text{Pb}$  and  $^{209}\text{Bi}$  at  $E_n = 800$  keV. The energy averaging increments are shown in keV and the average deviation between calculation and measurement is given in percent.

(Neg. ANL No. 116-76-242)

Fig. 6. Real potential depth as a function of target mass. Square and circular data points indicate the noted averaging increments. Solid data points are from the extended  $^{209}\text{Bi}$  data set described in the text.

(Neg. ANL No. 116-76-243)

Fig. 7. Real potential strength,  $VR^2$ , as function of mass. Notation is the same as in Fig. 6 with the addition of values at  $A \sim 207.25$  obtained from "elemental" lead constructed from the  $^{206}\text{Pb}$ ,  $^{207}\text{Pb}$  and  $^{208}\text{Pb}$  isotopes as described in the text.

(Neg. ANL No. 116-76-239)

Fig. 8. Comparison of measured and calculated differential elastic scattering cross sections of  $^{209}\text{Bi}$  at 8.05 MeV. Data points are taken from Holmqvist and Wiedling (22). The dashed curve indicates calculated results obtained with the potential of Ref. 22, based upon fits to high energy bismuth distributions. The solid curves were obtained using the present model.

(Neg. ANL No. 116-76-241)

Fig. 9. Comparison of measured and calculated  $^{238}\text{U}$  elastic and inelastic scattering cross sections at 0.55 MeV. Cross data points represent measured results of Barnard et al. (5), circular ones the results of Guenther et al. (6). The solid curves represent results obtained with the present potential as described in the text and the dashed curves were obtained with the potential of Ref. 19.

(Neg. ANL No. SFN 22-9)

Fig.10. Calculated and measured "elastic" scattering cross sections of  $^{238}\text{U}$  at 3.0 MeV. Data values are from Guenther et al. (X, 6) and from Batchelor et al. (O, 7). The light curve was obtained using the potential of Ref. 19 and the heavy curve the potential of the text. In both measurements and calculations it was assumed that the "elastic" distribution was inclusive of the 45 keV (2+) inelastic component.

(Neg. ANL No. 116-76-238)

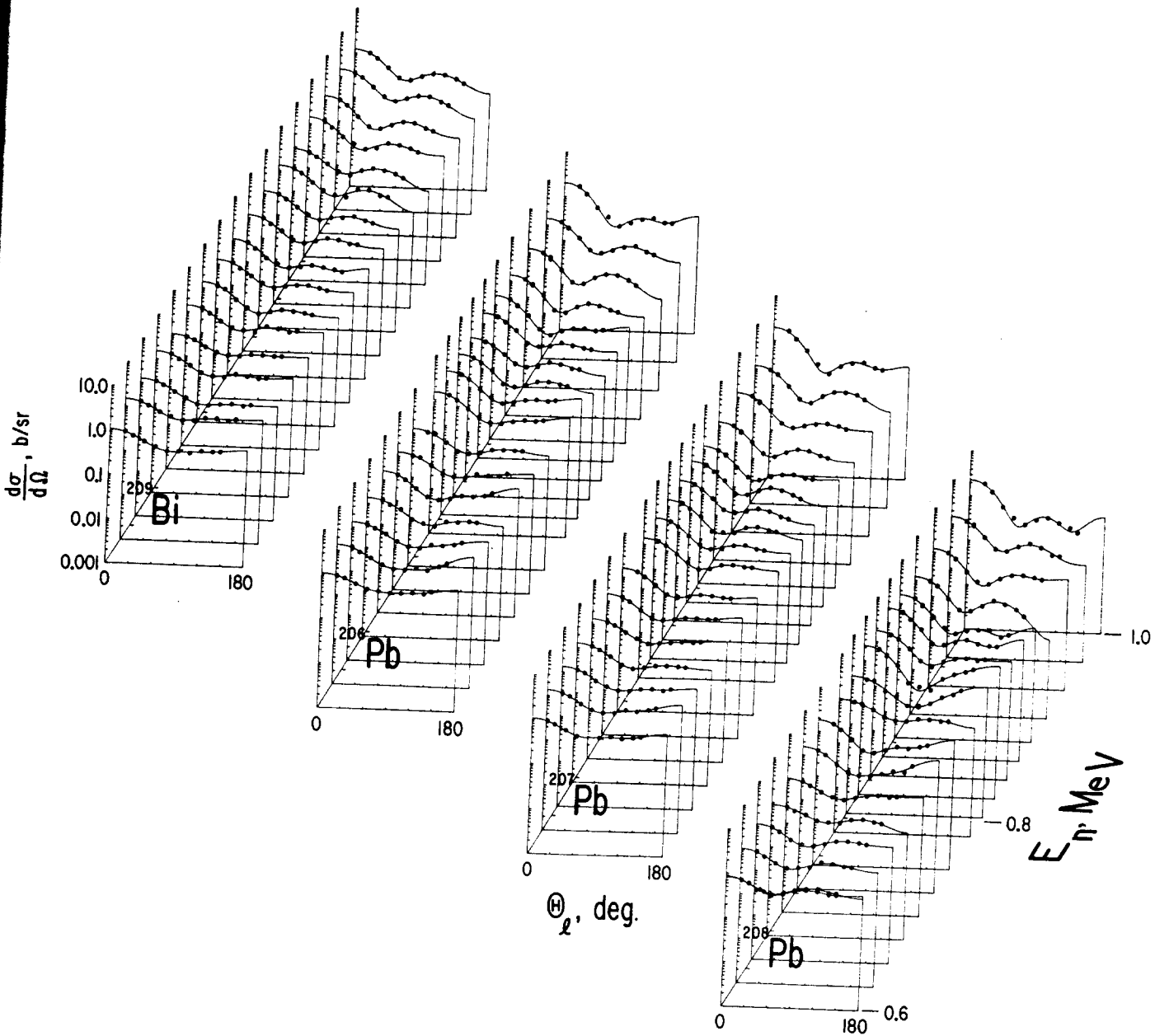


Fig.1

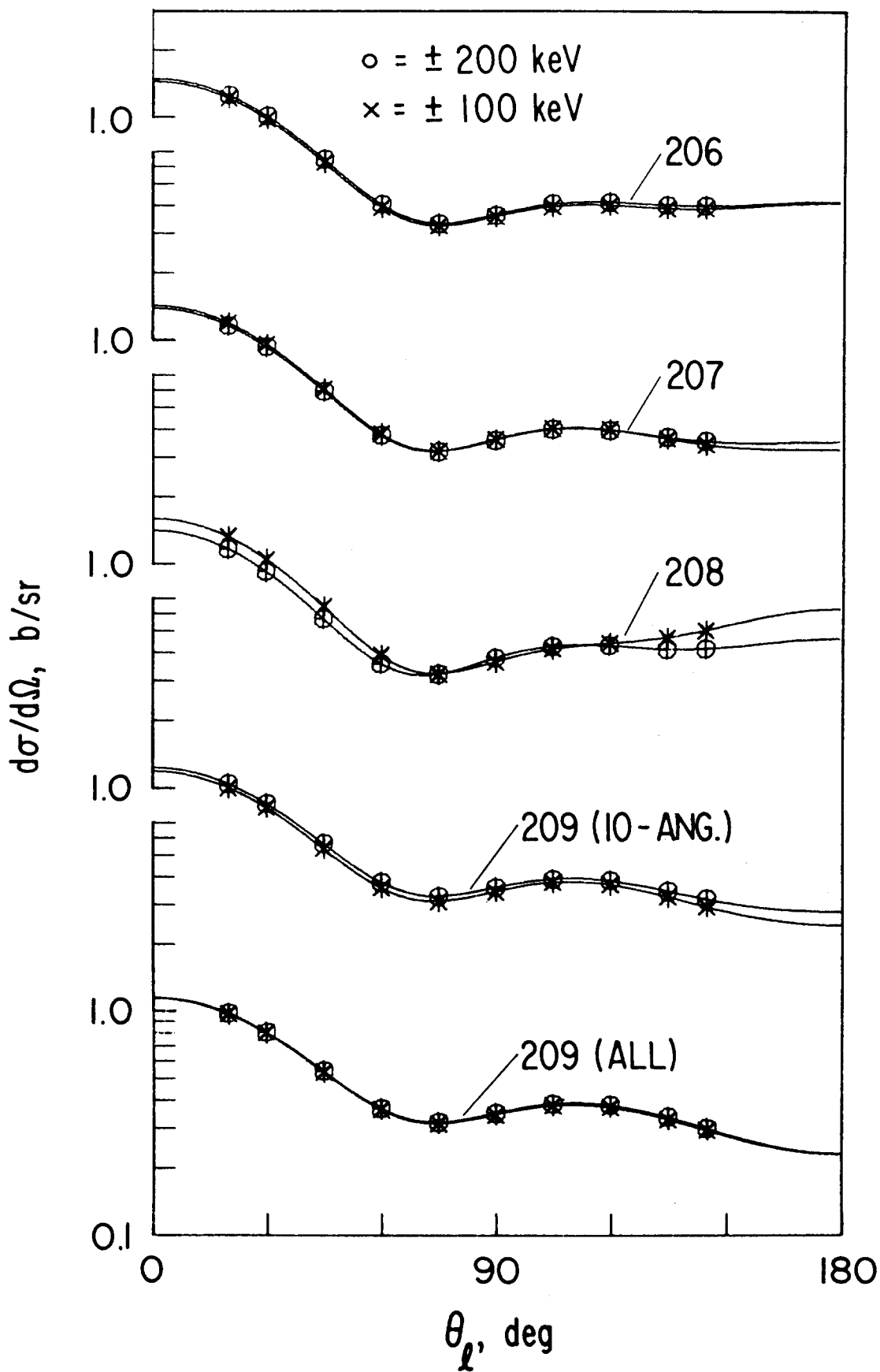
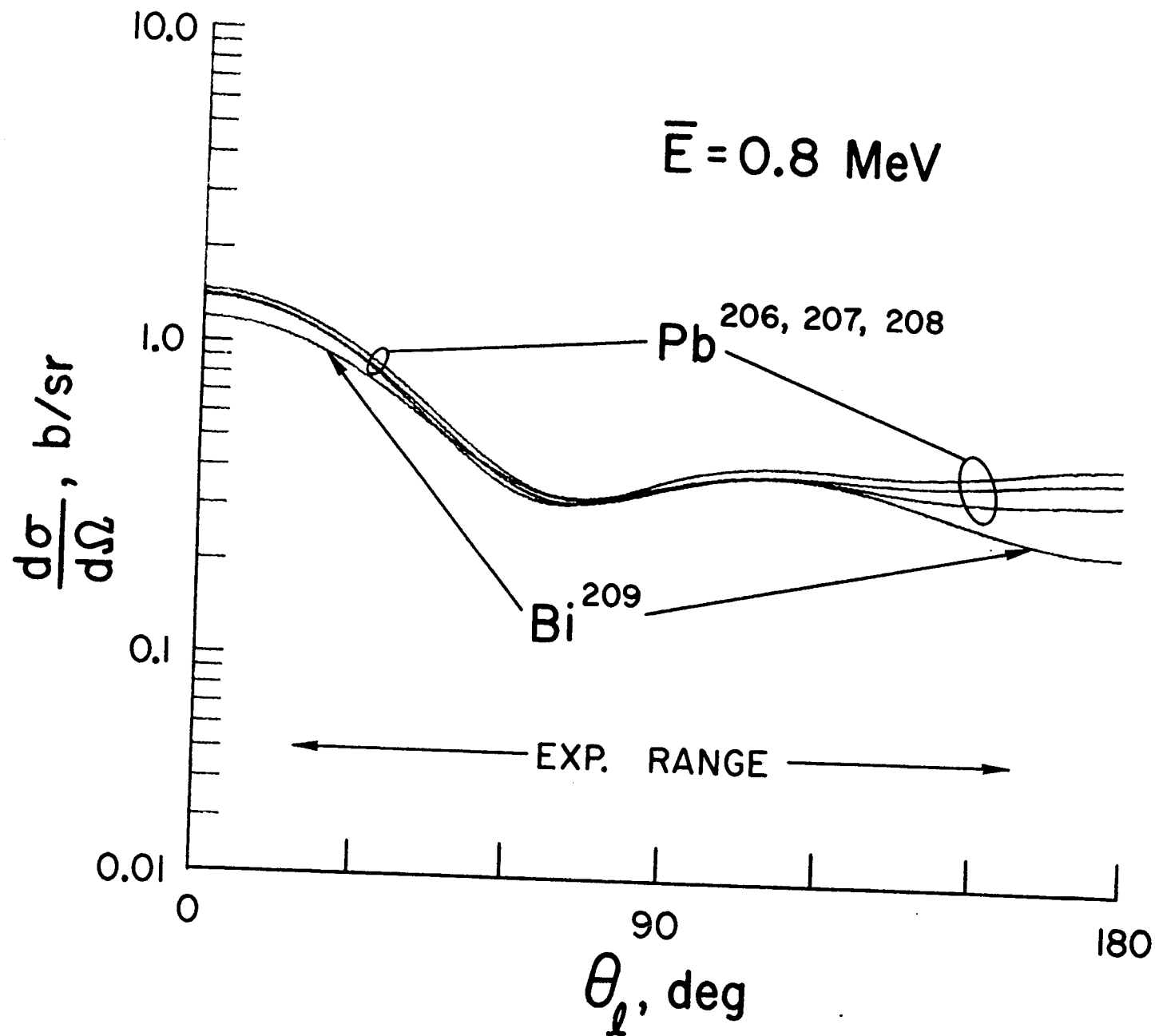


Fig.2

Fig. 3



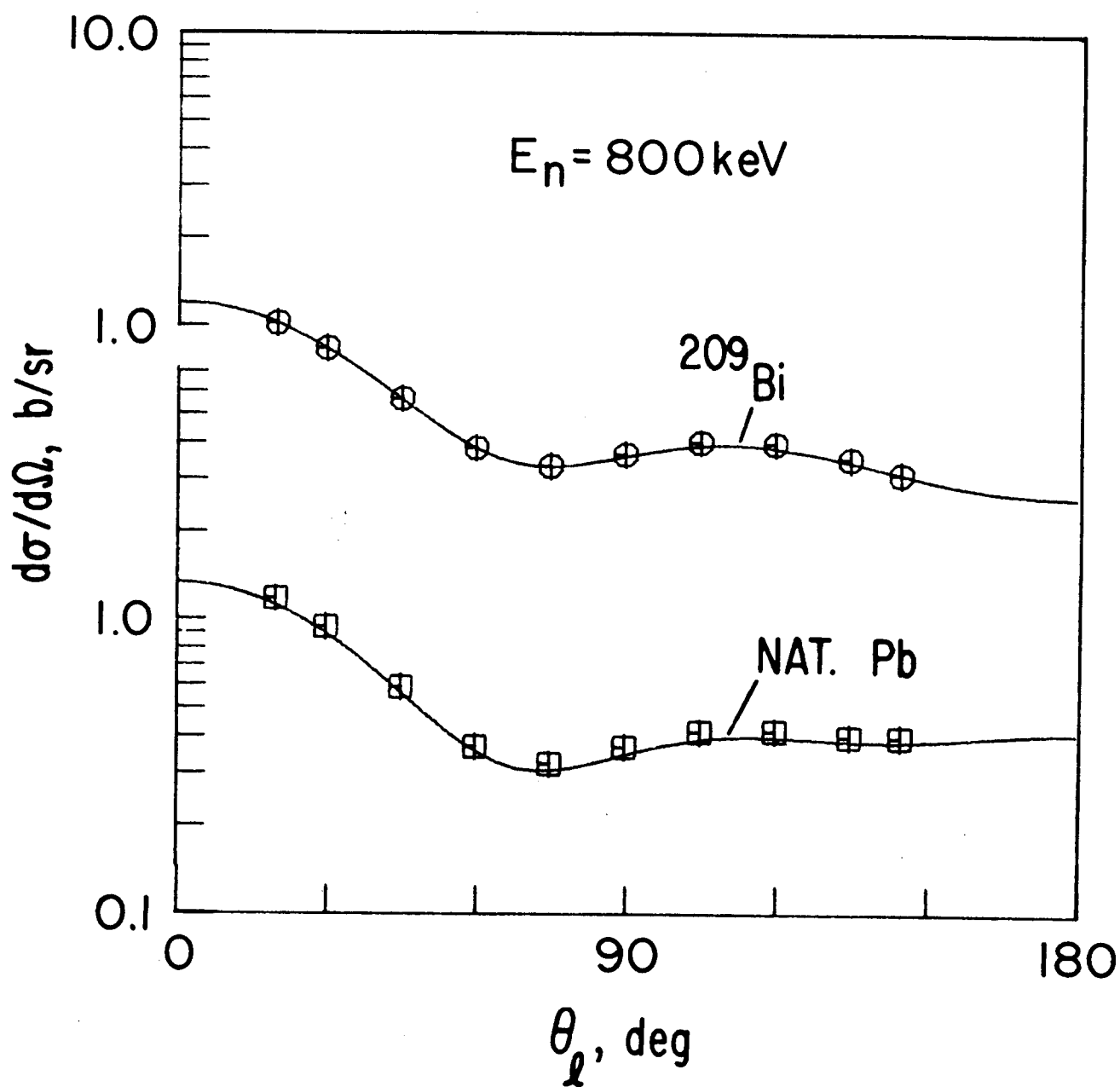


Fig.4

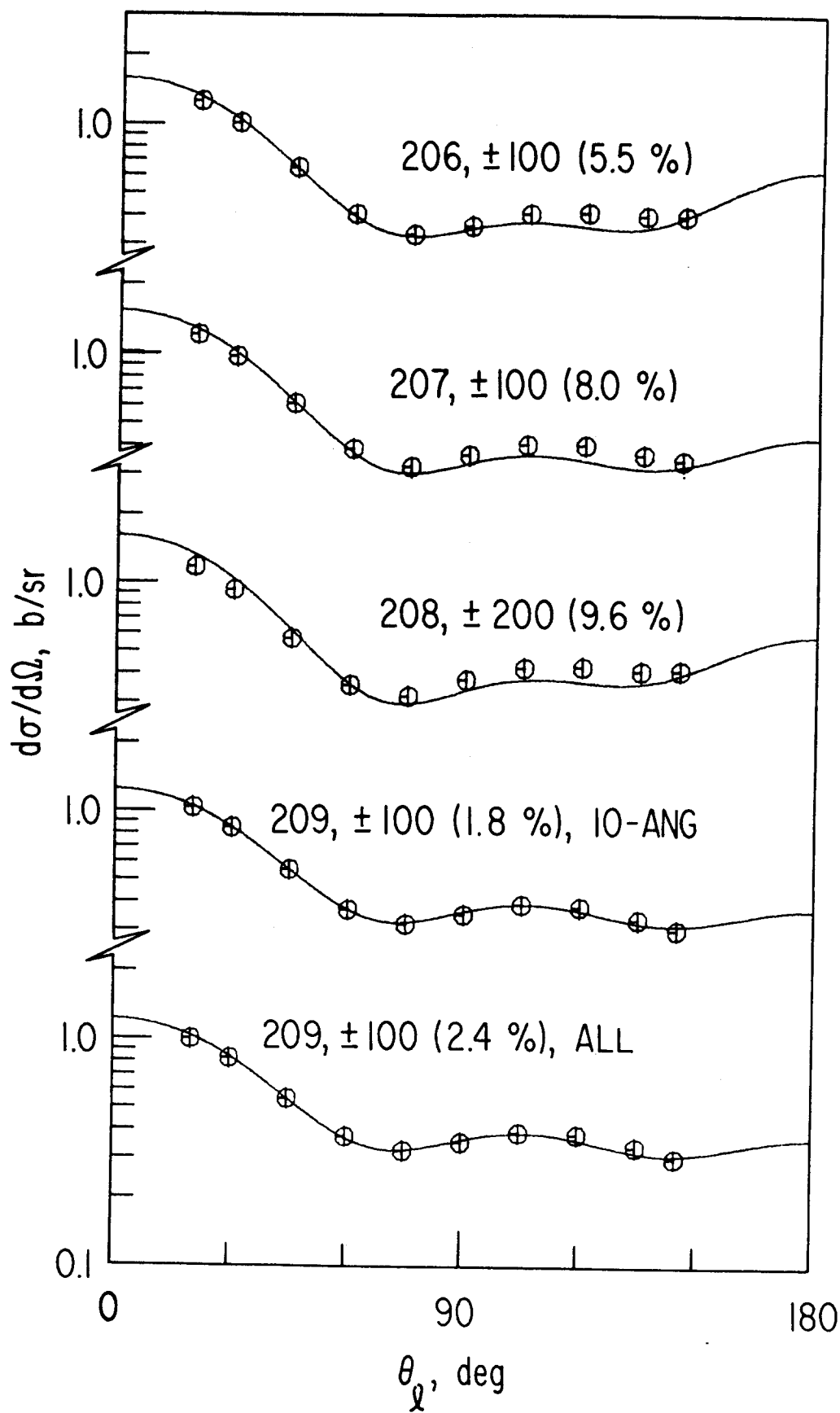


Fig.5

Fig. 6

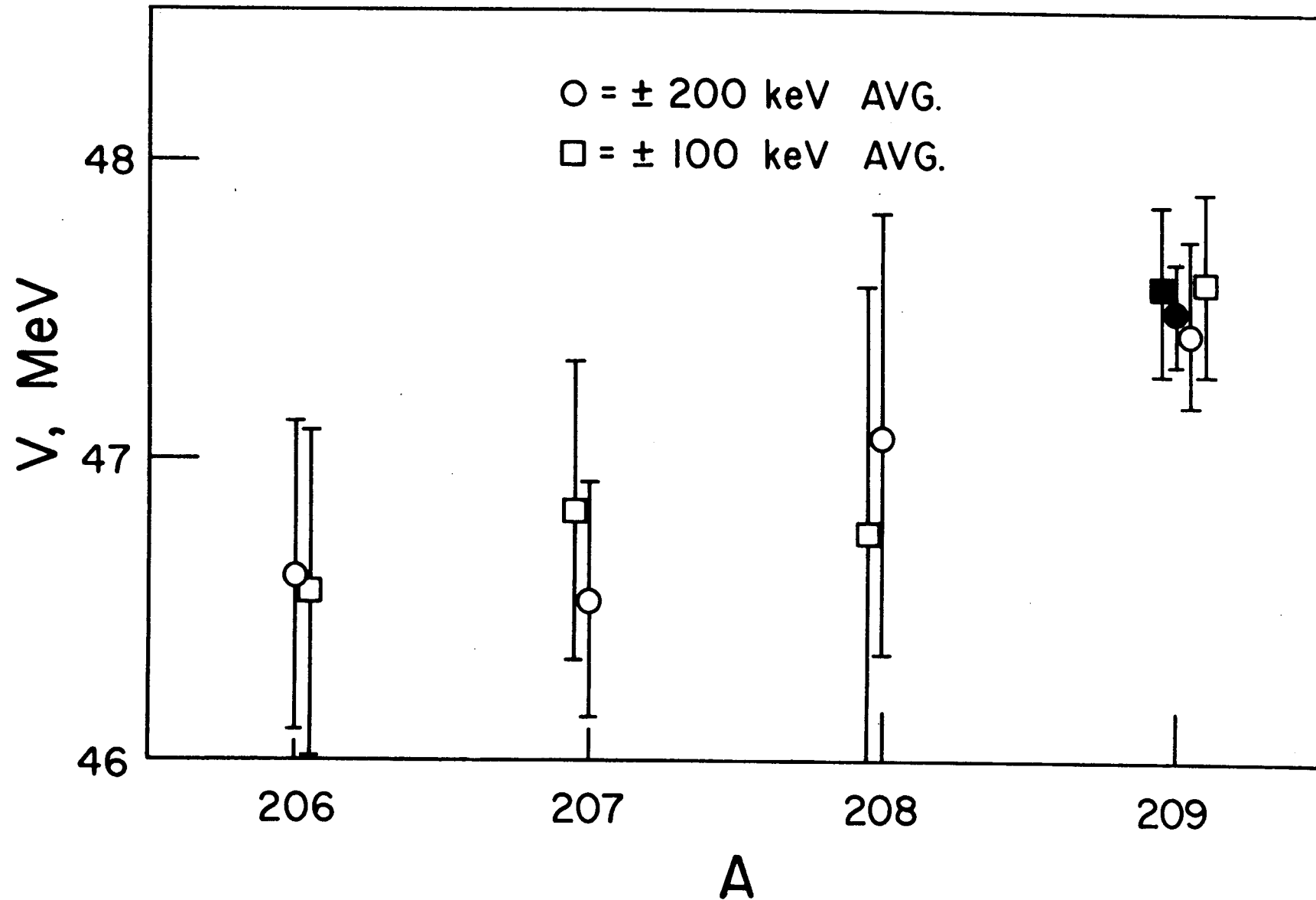
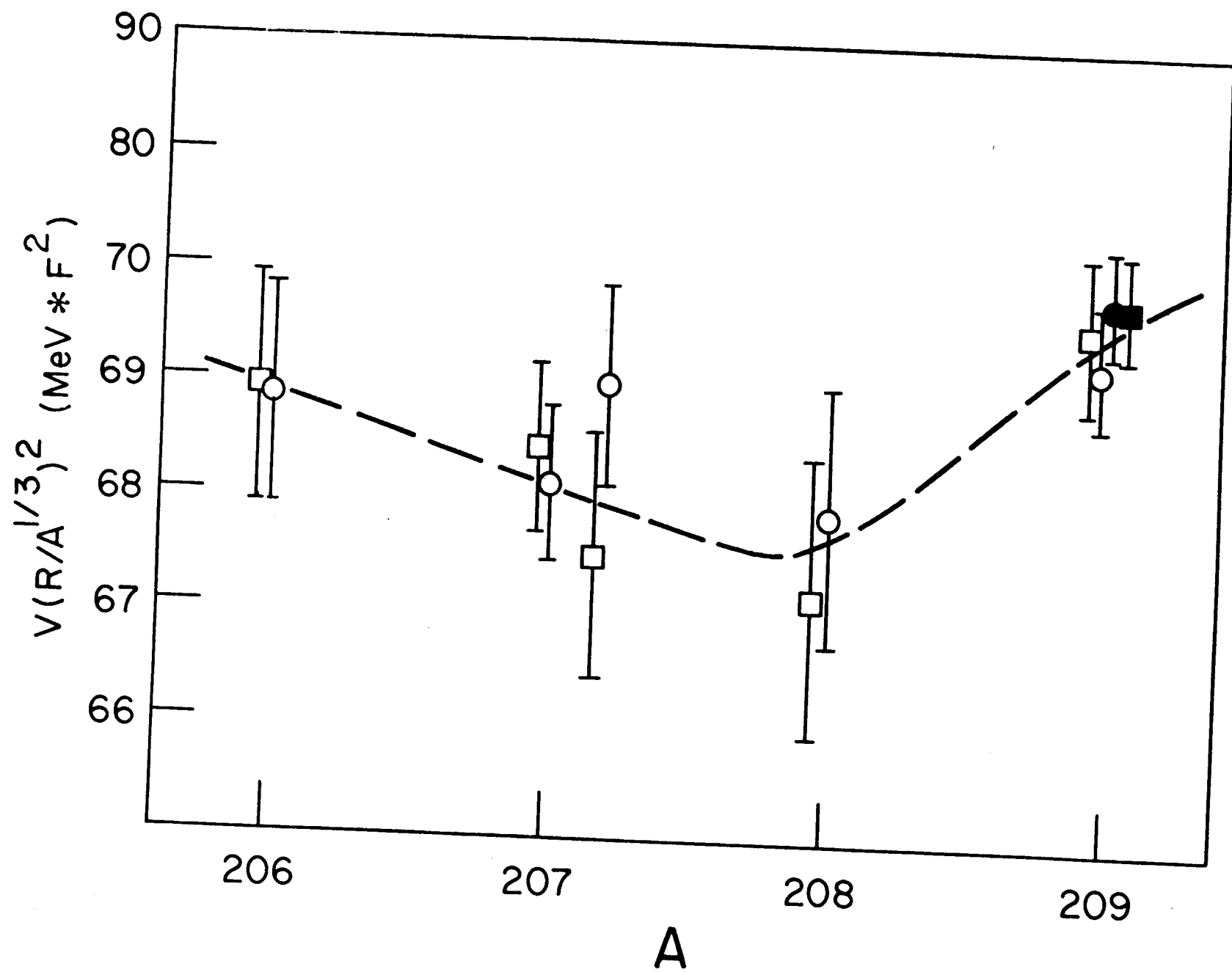


Fig. 7



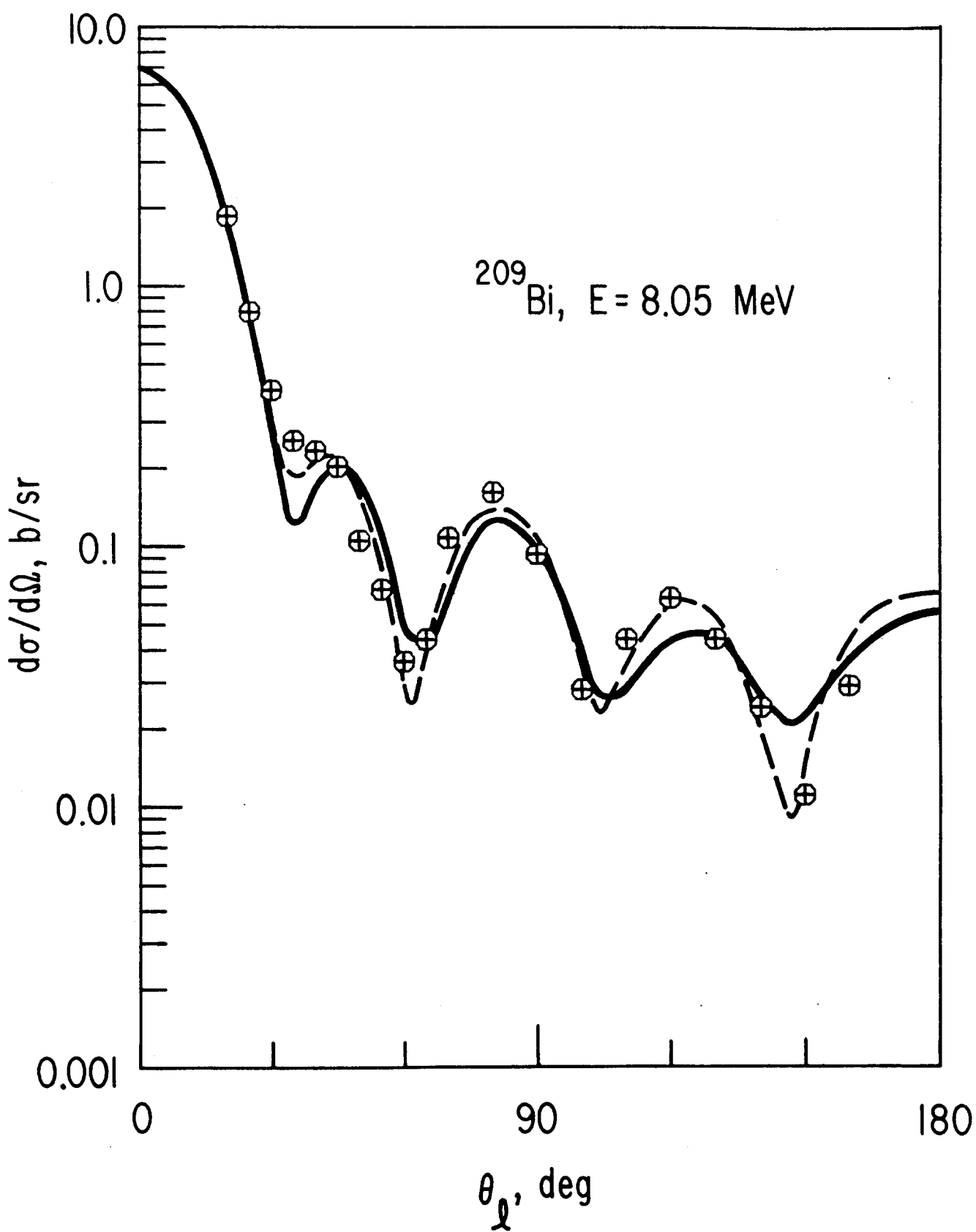


Fig.8

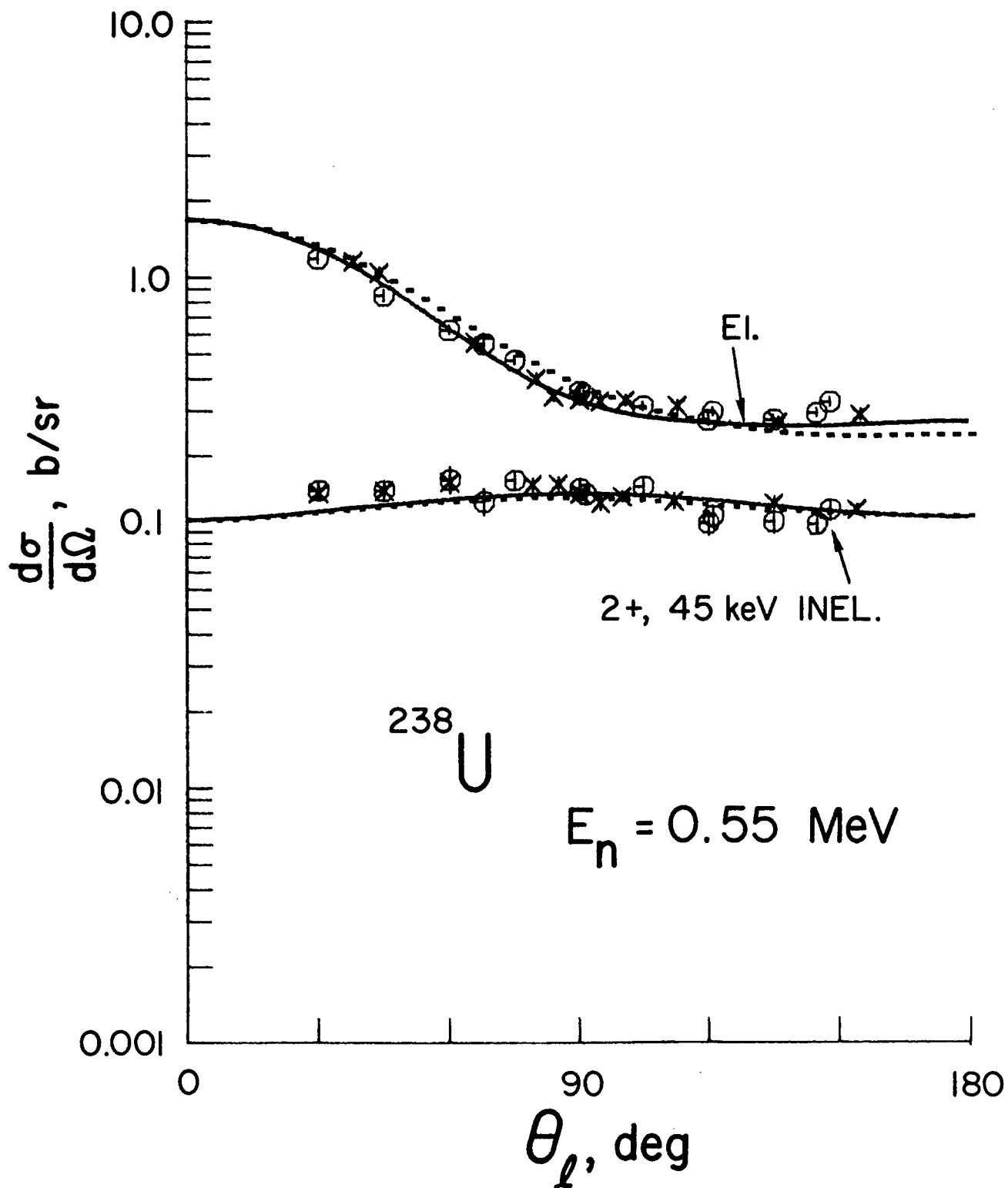


Fig.9

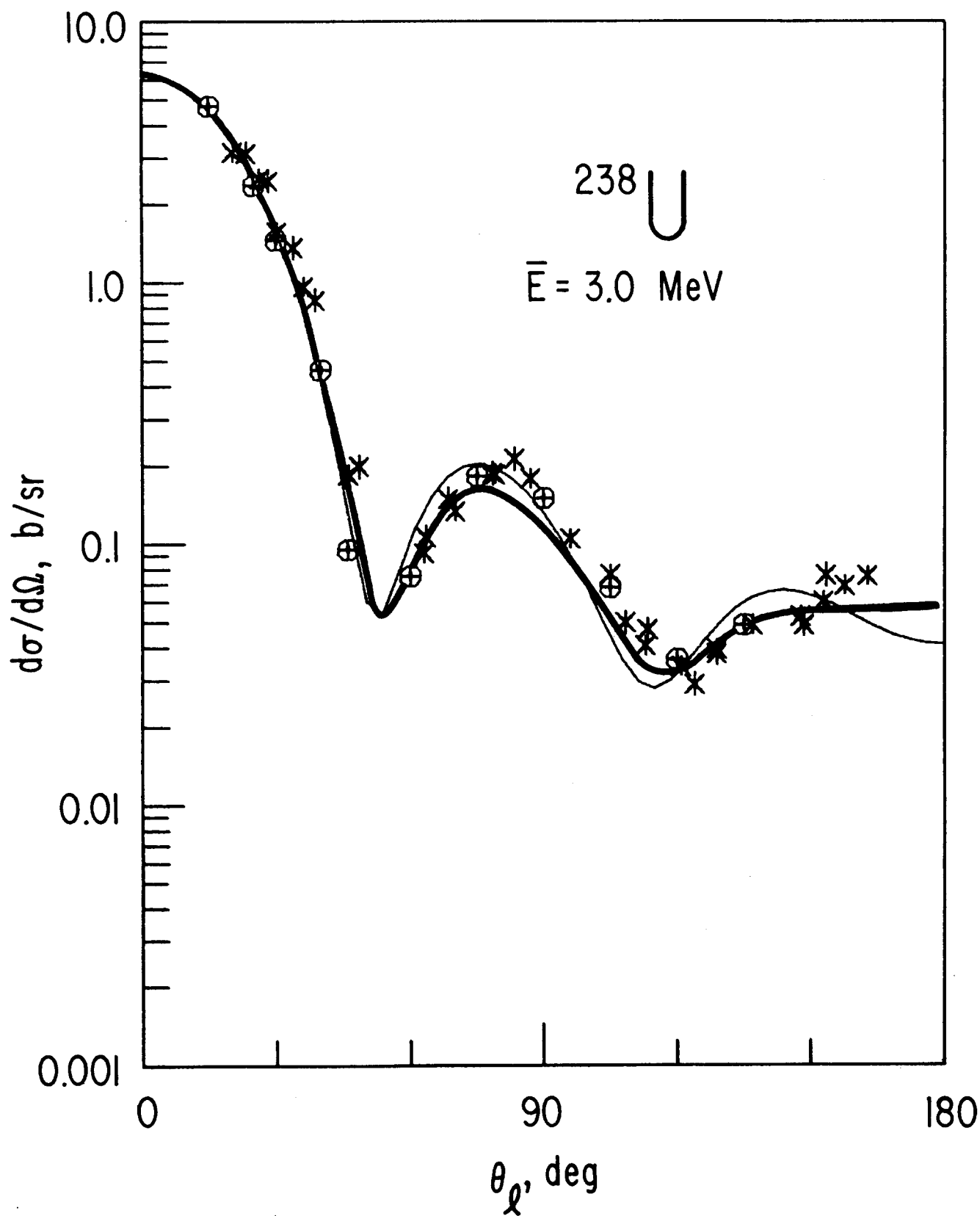


Fig.10